Icarus 202 (2009) 444–452

Contents lists available at ScienceDirect

Icarus

www.elsevier.com/locate/icarus

THEMIS observations of Mars aerosol optical depth from 2002–2008

Michael D. Smith

NASA Goddard Space Flight Center, Greenbelt, MD 20771, USA

ARTICLE INFO

Article history:
Received 23 January 2009
Revised 18 March 2009
Accepted 21 March 2009
Available online 25 March 2009

Keywords:
Mars, atmosphere
Mars, climate
Atmospheres, structure

ABSTRACT

We use infrared images obtained by the Thermal Emission Imaging System (THEMIS) instrument on-board Mars Odyssey to retrieve the optical depth of dust and water ice aerosols over more than 3.5 martian years between February 2002 (MY 25, $L_s = 330°$) and December 2008 (MY 29, $L_s = 183°$). These data provide an important bridge between earlier TES observations and recent observations from Mars Express and Mars Reconnaissance Orbiter. An improvement to our earlier retrieval [Smith, M.D., Bandfield, J.L., Christensen, P.R., Richardson, M.I., 2003. J. Geophys. Res. 108, doi:10.1029/2003JE002114] to include atmospheric temperature information from THEMIS Band 10 observations leads to much improved retrievals during the largest dust storms. The new retrievals show moderate dust storm activity during Mars Years 26 and 27, although details of the strength and timing of dust storms is different from year to year. A planet-encircling dust storm event was observed during Mars Year 28 near Southern Hemisphere Summer solstice. A belt of low-latitude water ice clouds was observed during the aphelion season during each year, Mars Years 26 through 29. The optical depth of water ice clouds is somewhat higher in the THEMIS retrievals at ~5:00 PM local time than in the TES retrievals at ~2:00 PM, suggestive of possible local time variation of clouds.

Published by Elsevier Inc.

1. Introduction

The continued successful operation of the Thermal Emission Imaging System (THEMIS) instrument on-board the Mars Odyssey spacecraft has allowed for the long-term monitoring of the Mars atmosphere for more than 3.5 martian years (Christensen et al., 2003). The atmosphere has been studied using both the visible and the infrared portions of the THEMIS instrument. Thermal infrared observations made by THEMIS in nine spectral bands enable the retrieval of the spatial and seasonal variation of dust and water ice column-integrated aerosol optical depth, as well as surface temperature and a vertically-averaged atmospheric temperature (Smith et al., 2003). THEMIS visible images have been used to characterize the morphology and seasonal dependence of dust and ice clouds (Inada et al., 2007), and to characterize mesoscale clouds (McConnochie et al., 2006).

The retrievals of aerosol optical depth from THEMIS observations provide a crucial link between the observations of aerosols taken by the Mars Global Surveyor TES (e.g. Smith, 2004) and Mars Orbiter Camera (MOC) instruments (e.g. Cantor et al., 2001; Cantor, 2007) and those taken by instruments on-board the currently-operating Mars Reconnaissance Orbiter (MRO) (e.g. Wolff et al., 2009) and Mars Express (MEx) orbiter (e.g. Zasova et al., 2005; Rannou et al., 2006). The long overlap in time (more than one martian year) between the THEMIS observations and both MGS and MRO/MEx observations provides an opportunity for the validation and cross-calibration between all the different instruments. Together, these datasets now cover a period of more than five martian years, enabling the initial exploration of interannual variations in atmospheric conditions.

The retrieval of dust and water ice aerosol optical depth using THEMIS infrared observations was previously described by Smith et al. (2003), and more information on the THEMIS instrument can be found in Christensen et al. (2003). A recent review of all previous spacecraft observations of aerosols in the martian atmosphere is also given by Smith (2008). In this paper, we describe improvements to the Smith et al. (2003) retrieval as well as results updated to the current time. In Section 2 we describe the set of THEMIS observations used in the retrieval of aerosol optical depth. In Section 3 we describe the retrieval algorithm, focusing on the improvements that have been made to the Smith et al. (2003) algorithm. In Section 4 we present the results of the retrieval along with a discussion of results, and we summarize our findings in Section 5.

2. Data set

2.1. THEMIS instrument

The THEMIS instrument obtains images of Mars using one of two separate focal planes. One focal plane contains ten spectral filters covering the thermal infrared between 6.5 and 15 μm, while

E-mail address: michael.d.smith@nasa.gov.

0019-1035/$ – see front matter Published by Elsevier Inc.
doi:10.1016/j.icarus.2009.03.027

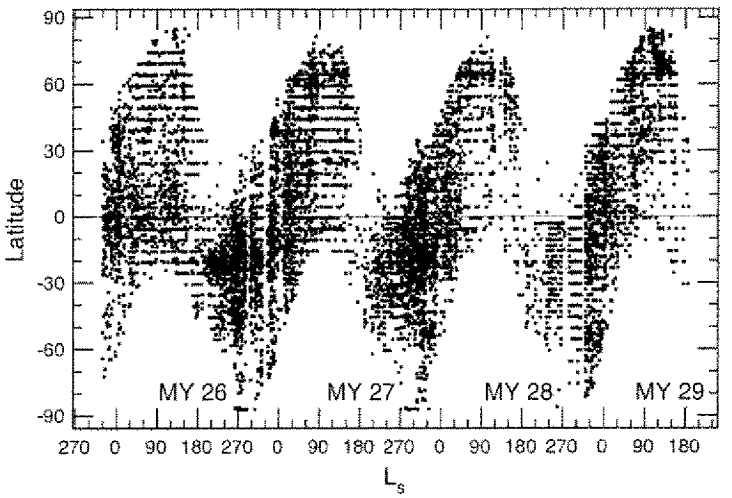

Fig. 1. The distribution in season (L_s) and latitude of the THEMIS retrievals of aerosol optical depth. There is nearly-continuous coverage for more than 3.5 martian years. Small gaps in coverage are caused by solar conjunction and spacecraft anomalies.

the other contains five spectral filters at visible wavelengths between 0.45 and 0.85 μm (Christensen et al., 2003). In this work we use only the images taken in the thermal infrared. The first two THEMIS spectral bands are identical and are centered at 6.78 μm. Bands 3 through 10 are centered at 7.93, 8.56, 9.35, 10.21, 11.04, 11.79, 12.57, and 14.88 μm, respectively, with spectral widths that allow for slight overlaps between adjacent bands (except for Band 10, which is somewhat more narrow and has no spectral overlap with any other band).

The THEMIS images are 320 pixels across-track and are built up in the along-track direction over time by spacecraft motion. Images are of variable length depending on the purpose of the observation and the available resources available for downlink of the data. The size of a THEMIS pixel at the surface is 100 m. The local time of the THEMIS observations varies between roughly 4:00 and 6:00 PM, which is somewhat later than either the 2:00 PM mean local time of Mars Global Surveyor or the 3:00 PM mean local time of the Mars Reconnaissance Orbiter.

We are most interested in the variations of atmospheric conditions on scales larger than the THEMIS pixel size, so for each THEMIS image we use as our observation the average of a block of data 320 pixels wide (the entire width of the image) by 256 pixels long. The last 256 pixels of each image are used for this average because they have the most accurate calibration (an effect only noticeable for Band 10). The resulting average covers an area 32 by 26 km in size, or roughly one-half degree square.

2.2. Observations used in this study

THEMIS images are divided between those targeted at objects of geologic interest, general mapping of the entire surface, and a latitude–longitude grid of observations taken every couple weeks intended to survey atmospheric conditions. Although the targeted observations generally provide a reasonable global-scale sampling over time, the atmospheric grid has proven to be very useful as a means to "fill in" any spatial gaps in the coverage of targeted observations.

Included in this work are all THEMIS images that include all ten infrared bands and for which the surface is sufficiently warm (220 K or higher) to provide enough thermal contrast between surface and atmosphere to allow for a reliable retrieval. A total of 26,400 images fit these criteria, covering the period from the beginning of the mission in February 2002, or Mars Year (MY) 25, $L_s = 330°$, to the end of December 2008 (MY 29, $L_s = 183°$). Although the number of available images per day varies somewhat with time, the coverage is nearly continuous over these 3.5 martian years with only short interruptions caused by solar conjunction or spacecraft anomalies.

Fig. 1 shows the seasonal (L_s) and latitudinal coverage of the THEMIS infrared images used in this work. Although the THEMIS instrument cannot provide a continuous pole-to-pole mapping because of data rate constraints, the coverage is still more than sufficient to provide a valuable picture of the seasonal and spatial trends of atmospheric aerosol optical depth. In particular, the value of the atmospheric grids can easily be seen during the aphelion season ($L_s = 0°–180°$) when data rates have typically been low.

3. Revised retrieval algorithm

The retrieval used here is the same as Smith et al. (2003) algorithm, except modified to include atmospheric temperature information from the THEMIS observations themselves. Here we give a brief outline of Smith et al. (2003) algorithm, and in the next section we describe the revision to include temperature information from the THEMIS observations.

The basic idea of the THEMIS retrieval is to find the values for surface temperature and dust and water ice aerosol optical depth that provide the best fit between the computed and observed radiance spectra in THEMIS Bands 3–8 (roughly 8–12 μm). The three quantities, surface temperature, dust optical depth, and water ice optical depth are fit simultaneously by linearizing the solution for radiance about the current best guess and iterating until solution. Convergence typically occurs in less than five iterations.

Radiance is computed using a purely absorbing plane-parallel atmosphere. Thus, the optical depth values reported here should be considered as effective absorptive optical depth only, not full extinction optical depth that includes scattering. Numerical experiments show that extinction optical depth is roughly 1.3 times absorption optical depth for dust, and 1.5 times absorption optical depth for water ice aerosol (Smith, 2004).

The spectral dependence of optical depth for dust and water ice aerosols is taken from TES retrievals (Bandfield and Smith, 2003) and are assumed to be constant in space and time. Because surface emissivity has a spectral dependence that is very similar to that of dust aerosol over the THEMIS wavelengths, the two cannot be retrieved independently. Instead, TES results are used for the spectral

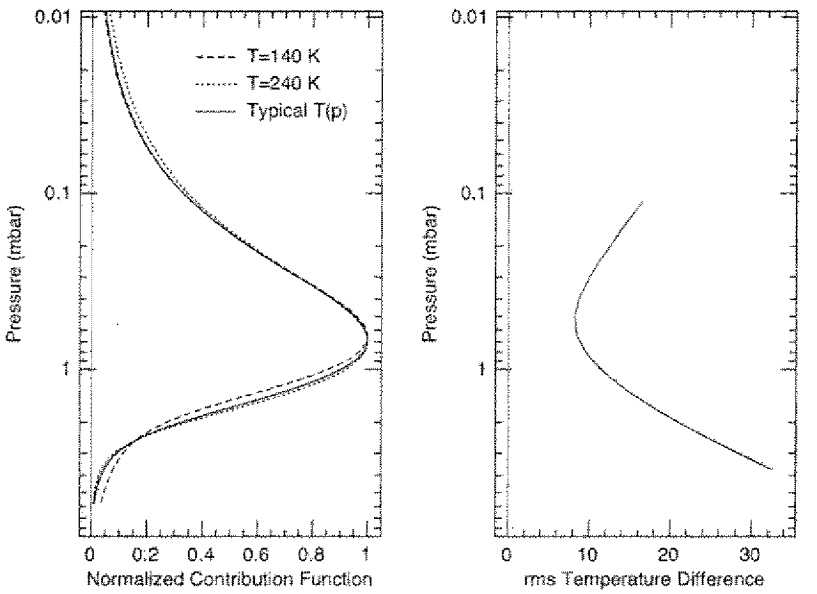

Fig. 2. Two determinations of the equivalent height represented by THEMIS Band 10 temperatures. (Left) Computed normalized contribution functions for a temperature profile typical of daytime conditions at low latitudes and $L_s = 180°$, and for two isothermal atmospheres bracketing expected martian conditions. (Right) Observed temperature differences between concurrent THEMIS Band 10 and TES retrieved temperatures at different pressure levels. Both methods indicate that THEMIS Band 10 is representative of a wide range of heights centered at about 0.5 mbar.

dependence of surface emissivity (Bandfield and Smith, 2003) and for the amplitude of surface emissivity as a function of latitude and longitude (Smith, 2004).

The vertical distribution of dust aerosol is assumed to be well-mixed. Water ice aerosol is assumed to be in the form of condensate clouds, so that there is no aerosol below the water condensation level. The condensation level is computed using a water vapor abundance taken from concurrent TES observations, or from TES climatology after the end of systematic TES spectrometer observations (MY 27, $L_s = 81°$).

3.1. Inclusion of THEMIS temperature information

The one THEMIS band sensitive to atmospheric temperature (Band 10) was designed to give a temperature representative of a broad range of the atmosphere (roughly 0.1–2.0 mbar), similar to the "T15" temperature derived from Viking Orbiter IRTM observations (Martin and Kieffer, 1979). Although useful, this single vertically-integrated temperature by itself is not sufficient to accurately model atmospheric radiance. The Smith et al. (2003) algorithm relied on concurrent retrievals from TES to provide the necessary temperature profiles. That strategy is no longer possible after the failure of the TES spectrometer (near-continuous observations by the TES spectrometer ended on 31 August 2004, or MY 27, $L_s = 81°$). For more recent THEMIS observations we use a combination of the averaged atmospheric temperature provided by THEMIS Band 10 with historic observations by TES at the same season and location (i.e. climatology) to estimate the temperature profile, $T(p)$, at the time of each THEMIS observation.

Although the temperature derived from THEMIS Band 10 is representative of a broad vertical range of the atmosphere, it is useful to define a single effective height for this temperature. Fig. 2 shows both a theoretical and an empirical derivation of this height. The left panel of Fig. 2 shows the contribution function for THEMIS Band 10 computed by taking the vertical derivative of the transmittance of the CO_2 atmosphere as a function of height integrated over the spectral response of THEMIS Band 10. The contribution function shows the vertical distribution of the relative contribution to the observed radiance in THEMIS Band 10. This distribution is not sensitive to the temperature profile as shown by the very similar contribution functions for three widely different temperature profiles. The peak of the contribution function is at a pressure level of about 0.6 mbar, although the peak is broad. The right panel of Fig. 2 shows the rms temperature difference between observed THEMIS Band 10 brightness temperatures and the temperatures at different pressure levels extracted from concurrent TES retrievals. This comparison includes all THEMIS observations taken during the period when the TES spectrometer was still operational, and so includes a complete range of seasons and latitudes. The minimum temperature difference is found at a pressure level of 0.5 mbar, which is in reasonable agreement with the theoretical results given the wide vertical distribution apparent from both methods. For the purpose of this retrieval, we assign an effective height of 0.5 mbar to the THEMIS retrievals.

Much of the time, using TES climatology temperatures for the THEMIS retrieval is a reasonable approximation. Fig. 3 shows a comparison between TES climatology temperatures at 0.5 mbar and observed THEMIS Band 10 temperatures. The TES climatology is taken from the first martian year of TES operations, from MY 24, $L_s = 104°$ to MY 25, $L_s = 104°$. There is excellent correspondence between the two during the aphelion season, $L_s = 0°$ to 180°. However, it is also apparent that the random timing and strength of large regional and planetary-scale dust storms during the perihelion season, $L_s = 180°$ to 360°, makes the use of TES climatology at those times much less desirable. These temperature differences can be quite large, exceeding 30 K for the largest dust storms. When actual atmospheric temperatures are greater than those predicted by TES climatology, then the thermal contrast between the surface and atmosphere will be overestimated, which means that aerosol optical depth will be underestimated.

It was noted by Smith (2004) that the atmospheric warming caused by dust storms varies with height. The largest response is at high altitudes, while there is little response at levels near the surface. Fig. 4 shows a time series of temperatures at low Southern latitudes from TES over three martian years for five different atmospheric levels. While there is large interannual variation from year

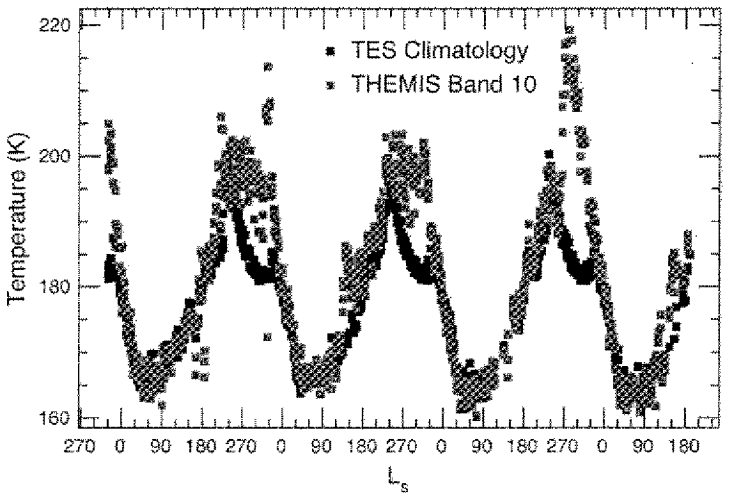

Fig. 3. A comparison of observed THEMIS Band 10 temperature against those estimated using TES climatology (at 0.5 mbar) from the first year of TES observations (MY 24 and 25). TES climatology provides a good estimate except when there are large dust storms.

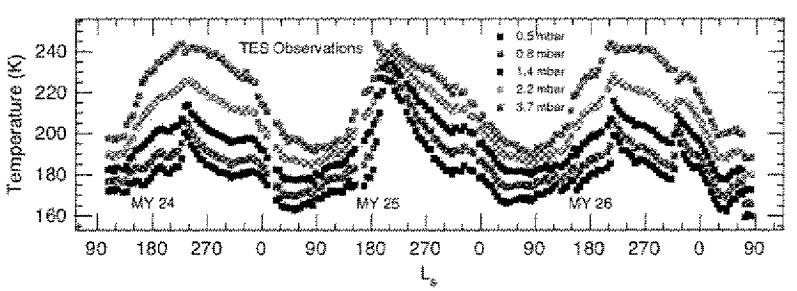

Fig. 4. Atmospheric temperatures retrieved from TES data as a function of season (L_s) and pressure level at a given location (20° S, 270° W). Variation in temperature from year to year in response to dust storms is most pronounced at greater heights above the surface and becomes relatively small near the surface.

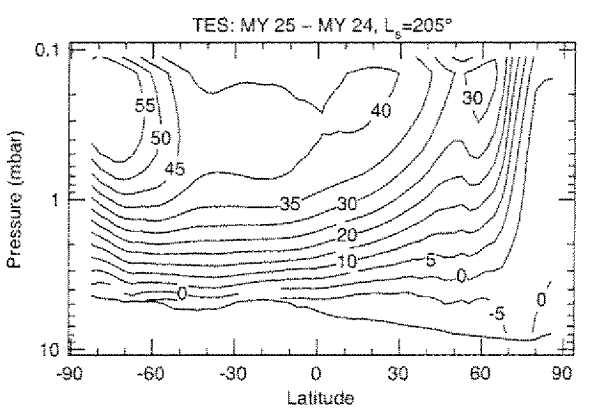

Fig. 5. The difference in zonally-averaged thermal structure of the martian atmosphere shown as a cross-section in latitude and log-pressure (the 0.1-mbar pressure level is ~40 km above the 6.1 mbar level) as observed by TES. The gently sloping line across the bottom indicates the zonally-averaged pressure at the surface. Shown is the change in the daytime temperatures as a result of the 2001 (MY 25) planet-encircling dust storm event. This is temperature at MY 25, $L_s = 205°$ (July 2001) minus the temperature at MY 24, $L_s = 205°$ (September 1999). The temperature difference rises almost linearly from near-zero at the surface to a maximum value somewhere above the 0.5-mbar level.

to year caused by dust storms at 0.5 mbar, the year-to-year variation near the surface (e.g., 3.7 mbar) is much reduced. Another example is given by Fig. 5, which shows the temperature difference as a function of latitude and height between temperatures observed by TES at MY 25, $L_s = 205°$ at the peak of a planet-encircling dust storm and those observed exactly one martian year previously when there was no dust storm (Smith et al., 2002). Here we see a near-zero temperature change at the surface increasing roughly linearly with height.

The TES observations of temperatures during dust storms suggest a relatively simple correction based on THEMIS Band 10 temperatures that can be made to improve the estimate of the temperature profile from TES climatology. We define a quantity, ΔT, as the difference between the observed THEMIS Band 10 temperature and the TES climatology temperature at 0.5 mbar (at the season, latitude, and longitude of the THEMIS observation). Recalling Fig. 3, most of the time ΔT is within 3 K of zero, but during dust storms ΔT becomes large and positive with values of 10–40 K. The temperature profile at the time of the THEMIS observation, $T(p)$, is then estimated from the TES climatology temperature profile, $T_{TES}(p)$, using:

$$T(p) = T_{TES}(p) + 0.4\,\Delta T \log \frac{p_{ref}}{p}, \tag{1}$$

where p_{ref} is a reference pressure level taken to be 6.1 mbar. Equation (1) provides a temperature correction that is zero at the reference pressure (essentially the surface) and increases linearly in log-pressure (nearly linear in height) to a value of ΔT at a pressure level of 0.5 mbar.

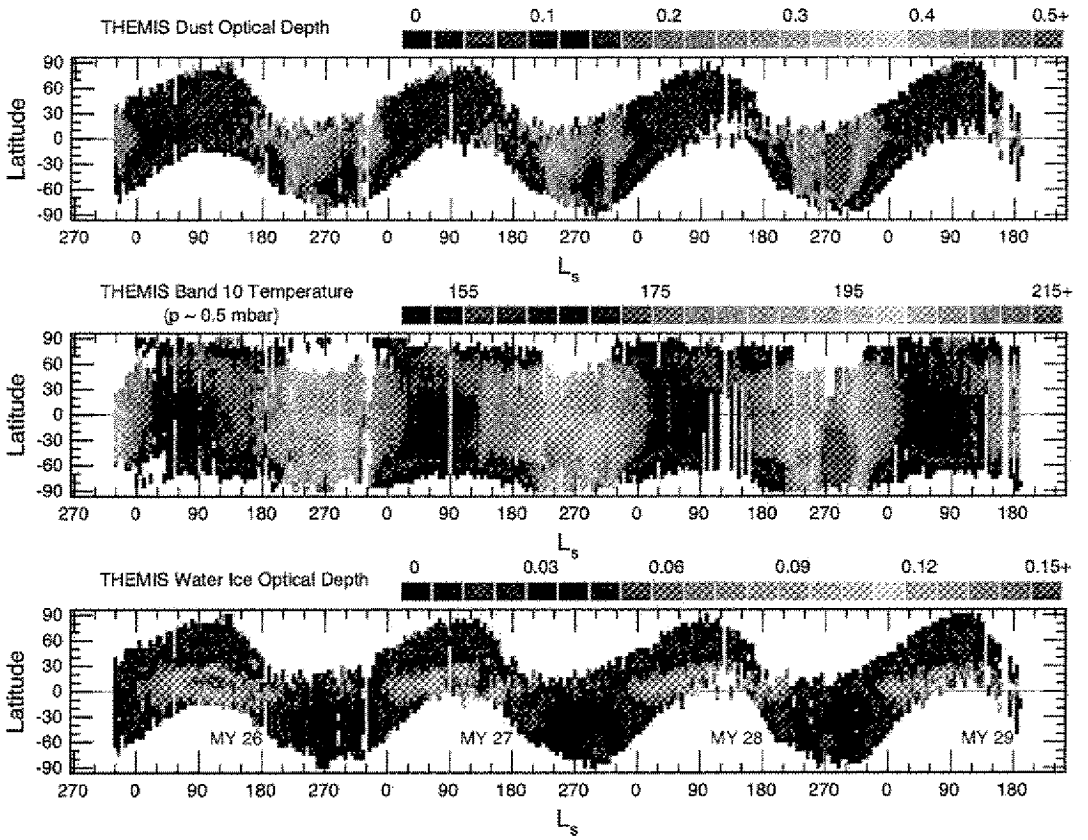

Fig. 6. An overview of THEMIS retrieved aerosol optical depth and Band 10 temperature over more than 3.5 martian years. Shown is the zonal average of each quantity as a function of season (L_s) and latitude. (Top) Dust optical depth at 1075 cm^{-1} scaled to an equivalent 6.1-mbar pressure surface to remove the effect of topography. (Middle) THEMIS Band 10 temperature, representative of a wide range of heights centered at about 0.5 mbar. (Bottom) Water ice optical depth at 825 cm^{-1}.

3.2. Estimation of uncertainties

A number of sources contribute to uncertainties in the retrieved values of dust and water ice optical depth, including instrument noise and calibration, error in the assumed temperature profile and surface emissivity, and simplifying assumptions of fixed spectral shapes and a well-mixed non-scattering aerosol. The formal propagation of random instrument noise leads to negligible error since we average over 320 × 256 pixel frames. Uncertainty from calibration and other systematic errors is not reduced by averaging pixels. Such uncertainties are difficult to evaluate, but our experience with the TES retrievals, and the comparison of THEMIS optical depth results with TES leads to an estimate of an uncertainty for a single THEMIS observation of 0.04 or 10% of the total absorption optical depth, whichever is larger. Uncertainties are likely somewhat higher (perhaps 20% or even greater) during the most intense dust storms because large corrections to the temperature profile must be made for those observations. The estimate for the uncertainty in optical depth also does not include the systematic difference between absorption and extinction optical depth. As stated earlier, we estimate that the extinction optical depth (including scattering) is systematically higher than the absorption optical depth reported here by ~30% for dust and ~50% for water ice.

4. Results

The retrieval of dust and water ice aerosol optical depth was performed on all THEMIS daytime infrared images with surface temperature greater than 220 K and all ten spectral bands present. The images span the entire 3.5 martian years of Mars Odyssey operations from MY 25, $L_s = 330°$ (19 February 2002) to the present, MY 29, $L_s = 183°$ (31 December 2008), yielding a total of 26,400 good retrievals.

Fig. 6 shows the results of our retrievals. Because dust has been assumed to be well-mixed, in Fig. 6 and the following figures we present dust optical depth scaled to an equivalent 6.1-mbar pressure surface to remove the effect of topography. This is accomplished by multiplying dust optical depth by the factor (6.1 mbar/surface pressure). Water ice aerosols have not been assumed to be well-mixed, and so we present water ice optical depth without any scaling. Band 10 temperatures are shown for all daytime infrared images without the restriction on surface temperature.

4.1. Dust optical depth

The history of dust optical depth shows the familiar seasonal dependence observed by previous spacecraft (Smith, 2008). The highest dust optical depth on a global scale is found during the perihelion season ($L_s = 180°$–$360°$), but with significant variation in the timing and amplitude of large dust storms from one martian year to the next. Relatively low dust optical depth persists throughout most of the aphelion season with the exception of occasional small-scale dust storms at high latitudes along the edge of the retreating polar ice caps.

The MY 26 dust storm season was relatively mild. As usual, dust activity began to pick up after $L_s = 140°$ with the first large regional storms at around $L_s = 210°$. Additional dust activity was

observed at high southern latitudes near summer solstice. The dust storms at $L_s = 315°$ are a regular feature of the dust cycle, but were noticeably more intense than those seen in previous years at that season (Liu et al., 2003; Smith, 2004). These dust storms were particularly notable since they occurred at the time of the Beagle 2 arrival at Mars, and just prior to the landings of two Mars Exploration Rovers (MER).

The MY 27 dust storm season was also mild, although there were several differences in the timing and intensity of the largest dust storm events compared with MY 26. An unusually early and intense low-latitude dust storm was observed in MY 27 at $L_s = 135°$, which was also observed at both MER landing sites by the rovers (Smith et al., 2006). However, this early activity was not followed up by increased dust optical depth during the rest of the season. Regional dust storms at $L_s = 225°$ were comparable in intensity although later than those observed in MY 26. The late-season dust activity at $L_s = 310°$ was more similar to the moderate dust storms observed in MY 24 and 25 by TES (Liu et al., 2003; Smith, 2004) than the more intense dust event of MY 26.

By far, the greatest dust activity observed so far by THEMIS occurred during MY 28. The early-season dust activity was not exceptional, with the regional dust activity at $L_s = 220°$ somewhat less intense than in previous years. However, at $L_s = 265°$ a series of dust storms began, which lead to a planet-encircling dust event. Thermal infrared dust optical depth exceeded unity over most of the planet for several weeks making this the highest global dust loading since the MY 25 (2001) event (Smith et al., 2002; Cantor, 2007). Dust optical depth only gradually decayed, staying above 0.5 until at least $L_s = 310°$. No new significant dust activity was observed by THEMIS during the usual $L_s = 310°$–$320°$ dust storm period, presumably because of the large perturbations of conditions from the late-season planet-encircling dust event.

Observations from THEMIS as we enter the dusty season for MY 29 once again show elevated early-season dust activity similar to that observed in MY 27.

4.2. THEMIS Band 10 temperatures

The middle panel of Fig. 6 shows THEMIS Band 10 brightness temperature, which was shown above in Section 3.1 to be a broad vertical average of atmospheric temperature with an effective height of roughly 0.5 mbar or 25 km above the surface. Atmospheric temperatures respond to a combination of orbital (perihelion vs. aphelion) and seasonal (summer vs. winter) variations, as well as to direct heating by the absorption of sunlight by dust and to general circulation patterns. The observed heating caused by the large regional storms during MY 26 and 27 was roughly 15–20 K, while that caused by the planet-encircling dust event of MY 28 was 30–40 K. Globally-averaged temperatures have a consistent and well-defined minimum near $L_s = 40°$, which is earlier than both aphelion ($L_s = 71°$) and the global minimum dust optical depth ($L_s = 130°$), a phenomenon also observed by TES (Smith, 2004).

4.3. Water ice optical depth

The main feature evident in the THEMIS retrievals of water ice aerosol optical depth (bottom panel of Fig. 6) is the aphelion season low-latitude cloud belt. This robust set of cloud features has been observed repeatedly by telescopic observations (e.g. Clancy et al., 1996), Viking (e.g. Tamppari et al., 2000), TES (Pearl et al., 2001; Liu et al., 2003; Smith, 2004), and other instruments. Low-latitude water ice optical depth increases rapidly after $L_s = 0°$ reaching its peak value by about $L_s = 60°$. The cloud-belt begins to dissipate after $L_s = 140°$ as atmospheric temperatures rise, but remnants persist until at least $L_s = 180°$. At its peak, there is significant cloud cover between 10° S latitude and 30° N latitude, with enhancements over areas of elevated topography such as Elysium, Tharsis, Olympus Mons, and Alba Patera. There is relatively little interannual variation in the timing, location, and amplitude of the cloud belt. However, the THEMIS observations do show that very early low-latitude dust storms, such as at MY 27, $L_s = 135°$, can very quickly reduce cloud optical depth to near-zero values. In this particular case, the cloud belt partially reformed by $L_s = 150°$ after the dissipation of the dust storm and atmospheric conditions had returned to nominal values for that season.

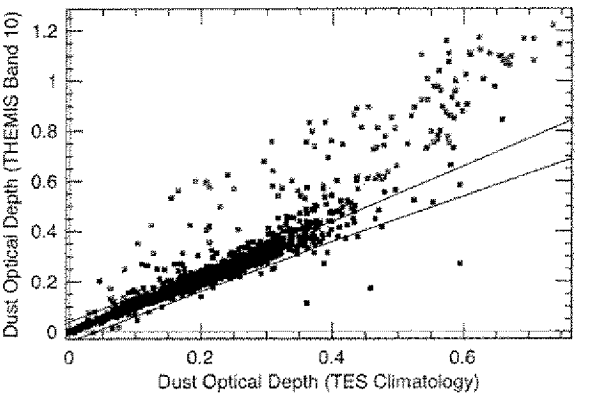

Fig. 7. A comparison of retrievals of dust optical depth from THEMIS observations using TES climatology and using THEMIS Band 10 information. The red points are those taken during the 2007 planet-encircling dust storm event (MY 28, L_s = 265°–305°).

The polar hood clouds that form at high latitudes in the winter hemisphere are not observed by THEMIS because at the relatively late local time of the Mars Odyssey orbit (~5:00 PM) surface temperatures are too low at those latitudes to provide the thermal contrast between the surface and atmosphere necessary for the reliable retrieval of water ice cloud optical depth.

4.4. Comparison against retrieval using TES climatology

The main difference between the original retrieval algorithm of aerosol optical depth from THEMIS infrared images used by Smith et al. (2003) and the algorithm used in this work is in how the atmospheric temperature profile is obtained. In the Smith et al. (2003) algorithm, concurrent TES observations were used to estimate atmospheric temperatures, but that is no longer possible since the end of systematic TES spectrometer observations on 31 August 2004 (MY 27, $L_s = 81°$). Instead, we estimate atmospheric temperatures using a combination of observed THEMIS Band 10 temperature and historic TES observations (climatology) from the season and location of interest.

Fig. 7 shows dust optical depth retrieved using observed THEMIS Band 10 temperature information compared to that retrieved using TES climatology alone without correction. In the figure, the red points are those observations taken during the 2007 planet-encircling dust storm event (MY 28, $L_s = 265°$–$305°$), while the black points are those taken at other times. The blue lines show when the two dust optical depth results are the same within uncertainties.

As expected, when there are no large dust storms the difference between retrieved dust optical depth using TES climatology and the correction using THEMIS Band 10 temperatures is essentially within the uncertainty of the algorithm. However, during large dust storms it is necessary to use observed THEMIS Band 10 temperatures to get an accurate retrieval. During large dust storms the observed THEMIS Band 10 temperature is higher than the climatology temperatures from the first year of TES observations (MY 24,

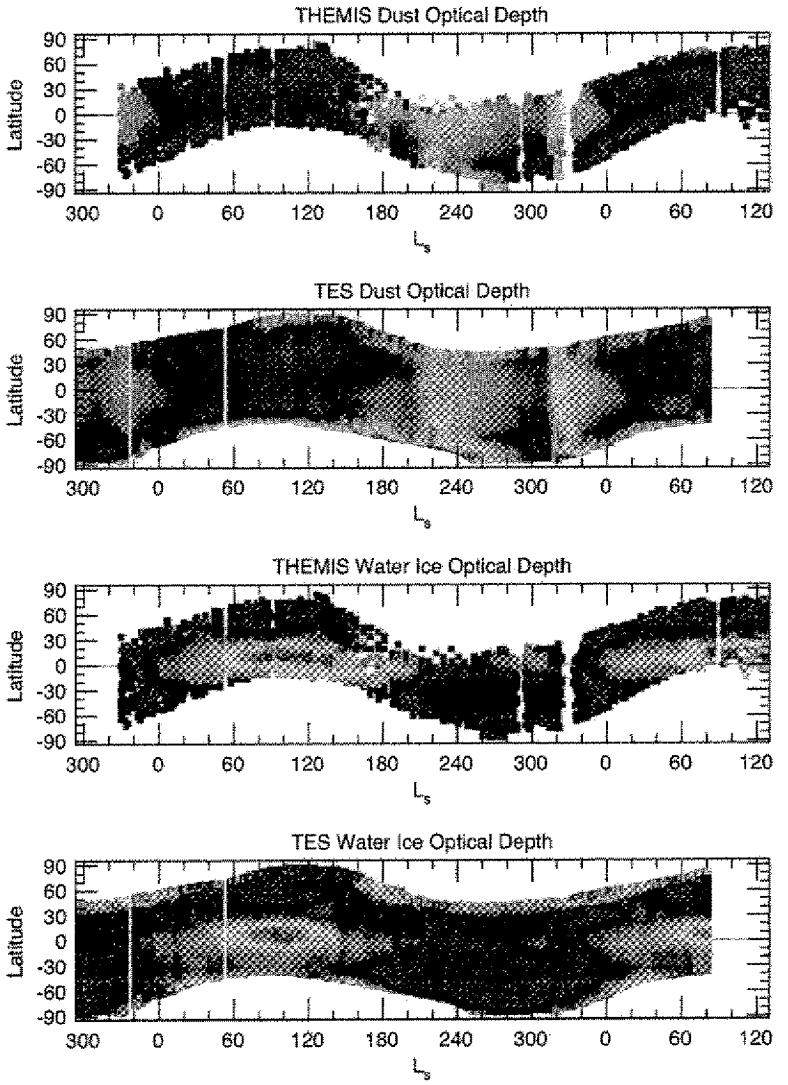

Fig. 8. A comparison of dust and water ice optical depth retrieved from THEMIS and TES observations during the time when both instruments were operational (MY 25, $L_s = 330°$ to MY 27, $L_s = 81°$). The scale for dust optical depth is from 0 (purple) to 0.5 (red). The scale for water ice optical depth is from 0 (purple) to 0.15 (red).

$L_s = 104°$ to MY 25, $L_s = 104°$), which was a very mild year for dust storms (Smith, 2004). Atmospheric temperatures greater than climatology lead to a smaller thermal contrast between the surface and atmosphere than would be expected from climatology. Therefore, to produce a spectral feature of a given size, a greater amount of dust must be present than would be required from atmospheric temperatures from climatology.

Fig. 7 shows that the above effect can be quite significant during the largest dust storms. The dust optical depth can be underestimated by up to a factor of two if observed temperatures are not used. Dust optical depth can also be underestimated by a smaller amount (10–20%) during large regional storms as shown by the upward curve of black points at larger values of dust optical depth.

4.5. Comparison against concurrent TES observations

Regular observations by the TES spectrometer continued for more than a martian year after the beginning of THEMIS observations allowing for a direct comparison between the two instruments and a validation of results from THEMIS. Fig. 8 shows side-by-side plots of dust and water ice optical depth retrieved from TES and THEMIS. The correspondence between the two is close, with both the seasonal and spatial patterns and the amplitudes of results matching well. Both TES and THEMIS observe the decay of a regional dust storm at the end of MY 25, the usual low dust optical depth during the aphelion season, and a relatively mild dusty season in MY 26 with moderate regional storms at $L_s = 210°$ and 315°. The aphelion season water ice cloud belt is observed by both instruments to begin intensification after $L_s = 0°$, reach full strength at $L_s = 60°$ with the same amplitude and latitude extent, and linger until about $L_s = 180°$.

One difference is the apparent cloudier conditions observed by THEMIS between $L_s = 120°$ and 180°. This was interpreted by Smith et al. (2003) as a result of the later local time of the THEMIS observations. Only one year (MY 26) in that seasonal period was observed by both TES and THEMIS concurrently. However, observations during this season for other years (MY 24 and 25 for TES; MY 27, 28, and 29 for THEMIS) show that during roughly $L_s = 100°$–180° the water ice optical depth observed by THEMIS is always somewhat higher than that observed by TES, ex-

cept for the sudden drop in clouds observed by THEMIS at MY 27, $L_s = 135°$ at the onset of an unusually early low-latitude dust storm. The difference in optical depth is about 0.03, which is close to the level of uncertainty. Nevertheless, the consistency of the trend over several years of observations from both instruments gives support to the idea that cloud optical depth varies with local time, a tendency also observed from telescopes (Wolff et al., 1999; Akabane et al., 2002; Glenar et al., 2003), Viking Orbiter (Tamppari et al., 2003), Mars Global Surveyor (Wilson et al., 2007), and Mars Reconnaissance Orbiter (Malin et al., 2008).

Notable in Fig. 8 is the smaller latitudinal range given by the THEMIS observations because of its later local time and thus cooler surface temperatures. This prevents the THEMIS observations from observing the polar hood water ice clouds seen by TES as well as some of the smaller dust storms along the edge of the polar caps. At the present time the Mars Odyssey spacecraft is performing maneuvers to move the local time of the orbit earlier, to about 3:00 PM. The move is expected to be complete in late 2009. This should provide a somewhat greater latitude extent for future aerosol optical depth retrievals, and may help provide a more definitive conclusion about the diurnal variation of water ice clouds in THEMIS observations.

5. Summary

Infrared images taken by the THEMIS instrument on-board Mars Odyssey are well-suited for the retrieval of dust and water ice optical depth in the Mars atmosphere. Use of atmospheric temperature information contained in THEMIS Band 10 data in the retrieval algorithm provides a much more accurate retrieval during large dust storms as compared to using temperatures from a climatology database alone. During the planet-encircling dust storm event of 2007 (MY 28), the observed THEMIS Band 10 atmospheric temperatures were 30 K warmer than those from TES climatology (Smith, 2004). Using a temperature profile based on the observed THEMIS Band 10 temperatures instead of directly from TES climatology resulted in an increase in retrieved dust optical depth during the storm by a factor of two or more.

The long and nearly-continuous record of THEMIS retrievals of aerosol optical depth provides a critical link between historic observations from Mars Global Surveyor data and the recent observations by the Mars Express and Mars Reconnaissance Orbiter spacecraft. Comparisons of aerosol optical depth retrieved from THEMIS and concurrent TES observations shows strong agreement providing a validation of the consistency of results from the two instruments. Similar cross-correlation and validation is currently underway comparing THEMIS retrievals against those from Mars Express and Mars Reconnaissance Orbiter instruments (e.g. Smith et al., 2009; Wolff et al., 2009).

Over a time span of more than 3.5 martian years, THEMIS observations have shown both repeatable patterns and large interannual variation in aerosol behavior. Mars Years 26 and 27 were observed to have moderate dust activity during the perihelion (southern spring and summer) season, with regional dust storms near $L_s = 220°$ and 315°, while MY 28 featured a planet-encircling dust storm event just before southern summer solstice but no late-season regional storm at $L_s = 315°$. Early season low-latitude dust storms were observed in both MY 27 and 29 before $L_s = 180°$, a type of event not observed by TES during MY 24–26.

The low-latitude aphelion season water ice cloud belt was observed each year from MY 26–29 to begin forming at $L_s = 0°$, reaching peak optical depth between $L_s = 100°$ and 120°, and gradually decay after $L_s = 140°$. Cloud thickness was observed to rapidly decline during the early-season dust storms in MY 27 and 29, and to recover to nominal values after dissipation of the dust storms.

The limited latitudinal extent of reliable THEMIS retrievals because of the late local time (~5:00 PM) of the Mars Odyssey orbit precluded the observation of both polar hood clouds and small dust storms along the edge of the polar caps. However, the later local time of THEMIS observations compared to TES (~2:00 PM) does allow for a limited examination of the variation of cloud optical depth with time of day. The THEMIS observations consistently show somewhat higher water ice optical depth in the low-latitude aphelion season cloud belt, especially after $L_s = 100°$.

The THEMIS instrument remains fully operational and continues to add to its long history of atmospheric observations. The Mars Odyssey spacecraft is currently undergoing maneuvers to bring the local time of its orbit to an earlier time. It is expected that the maneuvers will be completed in late 2009 with the orbit near 3:00 PM local time. Observations at the earlier time will allow the retrieval of aerosol optical depth over a greater latitude range and will provide further information on the time-of-day variation of water ice optical depth.

Acknowledgments

We thank the THEMIS operations team at Arizona State University for their expert acquisition, calibration, and handling of THEMIS data, and Phil Christensen for his continued support of THEMIS atmospheric observations and analysis. We thank Josh Bandfield for useful discussions about the THEMIS data and retrievals, and Michael Wolff and an anonymous referee for their helpful comments on this manuscript. This work was supported through the Participating Scientist program of the NASA Mars Odyssey project.

References

Akabane, A., Nakakushi, T., Iwasaki, K., Larson, S.M., 2002. Diurnal variation of martian water-ice clouds in Tharsis region of the low latitude cloud belt: Observations in 1995–1999 apparitions. Astron. Astophys. 384, 678–688.

Bandfield, J.L., Smith, M.D., 2003. Multiple emission angle surface–atmosphere separations of thermal emission spectrometer data. Icarus 161, 47–65.

Cantor, B.A., 2007. MOC observations of the 2001 Mars planet-encircling dust storm. Icarus 186, 60–96.

Cantor, B.A., James, P.B., Caplinger, M., Wolff, M.J., 2001. Martian dust storms: 1999 Mars orbiter camera observations. J. Geophys. Res. 106, 23653–26687.

Christensen, P.R., Jakosky, B.M., Kieffer, H.H., Malin, M.C., McSween, H.Y., Nealson, K., Mehall, G.L., Silverman, S.H., Ferry, S., Caplinger, M., Ravine, M., 2003. The Thermal Emission Imaging System (THEMIS) for the Mars 2001 Odyssey mission. Space Sci. Rev. 110, 85–130.

Clancy, R.T., Grossman, A.W., Wolff, M.J., James, P.B., Rudy, D.J., Billawalla, Y.N., Sandor, B.J., Lee, S.W., Muhleman, D.O., 1996. Water vapor saturation at low altitudes around Mars aphelion: A key to Mars climate? Icarus 122, 36–62.

Glenar, D.A., Samuelson, R.E., Pearl, J.C., Bjoraker, G.L., Blaney, D., 2003. Spectral imaging of martian water ice clouds and their diurnal behavior during the 1999 aphelion season. Icarus 161, 297–318.

Inada, A., Richardson, M.I., McConnochie, T.H., Strausberg, M.J., Wang, H., Bell III, J.F., 2007. High-resolution atmospheric observations by the Mars Odyssey Thermal Emission Imaging System. Icarus 192, 378–395.

Liu, J., Richardson, M.I., Wilson, R.J., 2003. An assessment of the global, seasonal, and interannual spacecraft record of martian climate in the thermal infrared. J. Geophys. Res. 108, doi:10.1029/2002JE001921.

Malin, M.C., Calvin, W.M., Cantor, B.A., Clancy, R.T., Haberle, R.M., James, P.B., Thomas, P.C., Wolff, M.J., Bell III, J.F., Lee, S.W., 2008. Climate, weather, and north polar observations from the Mars Reconnaissance Orbiter Mars Color Imager. Icarus 194, 501–512.

Martin, T.Z., Kieffer, H.H., 1979. Thermal infrared properties of the martian atmosphere, I. Geophys. Res. 84, 2843–2852.

McConnochie, T.H., Bell III, J.F., Savaransky, D., Wolff, M.J., Richardson, M.I., Toigo, A.D., Wang, H., Christensen, P.R., 2006. Martian mesospheric clouds: Latest results from THEMIS-VIS. In: AGU Fall Meeting 2006. Abstract P23A-0044.

Pearl, J.C., Smith, M.D., Conrath, B.J., Bandfield, J.L., Christensen, P.R., 2001. Observations of martian ice clouds by the Mars Global Surveyor Thermal Emission Spectrometer: The first martian year. J. Geophys. Res. 106, 12325–12338.

Rannou, P., Perrier, S., Bertaux, J.-L., Montmessin, F., Korablev, O., Rébérac, A., 2006. Dust and cloud detection at the Mars limb with MV scattered sunlight with SPICAM. J. Geophys. Res. 107, doi:10.1029/2006JE002693.

Smith, M.D., 2004. Interannual variability in TES atmospheric observations of Mars during 1999–2003. Icarus 167, 148–165.
Smith, M.D., 2008. Spacecraft observations of the martian atmosphere. Annu. Rev. Earth Planet. Sci. 36, 191–219.
Smith, M.D., Pearl, J.C., Conrath, B.J., Christensen, P.R., 2002. Thermal emission spectrometer observations of martian planet-encircling dust storm 2001a. Icarus 157, 259–263.
Smith, M.D., Bandfield, J.L., Christensen, P.R., Richardson, M.I., 2003. Thermal Emission Imaging System (THEMIS) infrared observations of atmospheric dust and water ice cloud optical depth. J. Geophys. Res. 108, doi:10.1029/2003JE002114.
Smith, M.D., Wolff, M.J., Spanovich, N., Ghosh, A., Canfield, D., Christensen, P.R., Landis, G.A., Squyres, S.W., 2006. One martian year of atmospheric observations using MER Mini-TES. J. Geophys. Res. 111, doi:10.1029/2006JE002770. E12S13.
Smith, M.D., Wolff, M.J., Clancy, R.T., Murchie, S.L., 2009. CRISM observations of water vapor and carbon monoxide. J. Geophys. Res., doi:10.1029/2008JE003288, in press.
Tamppari, L.K., Zurek, R.W., Paige, D.A., 2000. Viking-era water ice clouds. J. Geophys. Res. 105, 4087–4107.
Tamppari, L.K., Zurek, R.W., Paige, D.A., 2003. Viking-era diurnal water-ice clouds. J. Geophys. Res. 108 (E7), doi:10.1029/2002JE001911.
Wolff, M.J., Bell III, J.F., James, P.B., Clancy, R.T., Lee, S.L., 1999. Hubble space telescope observations of the martian aphelion cloud belt prior to the Pathfinder mission: Seasonal and interannual variations. J. Geophys. Res. 104 (E4), 9027–9041.
Wolff, M.J., Clancy, R.T., Smith, M.D., Arvidson, R., Kahre, M., Seelos IV, F., Morris, R.V., 2009. Wavelength dependence of dust aerosol single scattering albedo as observed by CRISM. J. Geophys. Res., doi:10.1029/2009JE003350, in press.
Wilson, R.J., Neumann, G.A., Smith, M.D., 2007. Diurnal variation and radiative influence of martian water ice clouds. Geophys. Res. Let. 34, doi:10.1029/2006GL027976. L02710.
Zasova, L., and 20 colleagues, 2005. Water clouds and dust aerosols observations with PFS MEX at Mars. Planet. Space Sci. 53, 1065–1077.